Quantum Electronics **49** (8) 788–795 (2019)

https://doi.org/10.1070/QEL16929

Characteristics of quasi-unipolar electromagnetic pulses formed in the interaction of high-power laser pulses with nanoscale targets*

V.V. Kulagin, V.N. Kornienko, V.A. Cherepenin, D.N. Gupta, H. Suk

Abstract. **A new method is suggested for generating quasi-unipolar electromagnetic IR and terahertz pulses. The method is based on synchronous acceleration of electrons combined to a dense bunch with a charge of up to several tens nanocoulombs, which are forced out from a nanoscale target under an action of a high-power, sharp-leading edge laser pulse. The electromagnetic bunch moving in a field of laser radiation can generate high-power electromagnetic pulses with various spectral composition including terahertz and IR ranges. A physical mechanism underlying the formation of generated quasi-unipolar pulses of electromagnetic radiation is determined and numerically studied. The pulse characteristics are found by numerical simulation, such as amplitude and duration dependences on the angle between the pulse propagation direction and laser beam axis. It is established that in modern laser installations, the amplitudes of quasi-unipolar pulses may reach relativistic values. Reflection of a unipolar pulse from an ideally reflecting surface is numerically analysed. It is shown that the pulse retains its unipolar profile in this case.**

Keywords: *interaction of high-power laser pulses with matter, electron acceleration by laser pulses, generation of terahertz and IR radiation, nanoscale targets.*

1. Introduction

The terahertz frequency range is between the IR and microwave ranges. Presently, studies on generation and application of terahertz-range radiation are actively developing [1, 2]. Terahertz radiation is widely used in remote probing, imaging of inner structure of objects, biological and medical diagnosing, study of material characteristics, terahertz spectroscopy, scientific investigations and other fields. Some applications require a large amplitude of terahertz pulses, in particular, investigation of nonlinear interaction in the terahertz frequency range and nonlinear terahertz spectroscopy, which will provide additional knowledge about properties of various systems including quantum structures and biological materials. One more application that is obvious is the employment of high-amplitude terahertz pulses for electron and ion acceleration, including formation of a composite accelerating field along with the laser pulse. In the latter case, terahertz pulses with a high amplitude may be preferable.

A great number of schemes have been suggested for generating terahertz pulses with various power and duration based on semiconductor materials, nonlinear optical crystals, plasma, gas and solid-state media [3–5]. Many of such schemes employ femtosecond lasers, for example, for photoswitching semiconductor structures, optical rectifying or parametric oscillation in nonlinear crystals, formation of a wakefield or filaments in gases, ionisation or excitation vibrations on a surface of a solid-state target, etc. The most promising for producing high-intensity terahertz fields are the approaches, which employ various physical effects related to interaction of high-power laser pulses with plasma [6–15], because in this case, there are no limitations due to the medium breakdown in a strong electromagnetic field. One more investigation field is the employment of solid-state nanoscale targets, which have a dimension in one (or several) direction of at most 100 nm. In the latter case, in certain conditions, quasi-neutrality of plasma may be broken, and electron bunches will be formed with charges of up to several tens nanocoulombs. Motion of such bunches in the field of a laser pulse may have a complicated character, and high-power electromagnetic pulses will be generated at various frequencies including terahertz and IR ranges [16, 17].

An example of nanoscale targets are nanofilms widely used in laser-plasma experiments, which may have a thickness of several nanometres and a transverse size of hundreds micrometres. At normal incidence of a high-power non-adiabatic laser pulse to such a target, synchronous extrusion of all electrons from the nanofilm may occur in the wavevector direction under the action of a longitudinal (along the laser beam axis) Lorentz force component; the electron velocity in this case reaches relativistic values [18, 19]. First experiments on generation of relativistic electron bunches from nanofilms approved realisation of this scenario [20–22]. However, the efficiency of emission by the whole electron ensemble in this case is low, because conventionally, a transverse size of the film is greater than the laser beam diameter. The field related to charge separation is con-

*Presented at the UltrafastLight-2018 Conference, Moscow, October 2018).

V.V. Kulagin Sternberg Astronomical Institute, M.V. Lomonosov Moscow State University, Universitetsky prosp. 13, 119991 Moscow, Russia; Kotel'nikov Institute of Radioengineering and Electronics, Russian Academy of Sciences, ul. Mokhovaya 11, 125009 Moscow, Russia; e-mail: victorvkulagin@yandex.ru;
V.N. Kornienko, V.A. Cherepenin Kotel'nikov Institute of Radioengineering and Electronics, Russian Academy of Sciences, ul. Mokhovaya 11, 125009 Moscow, Russia;
D.N. Gupta Department of Physics and Astrophysics, University of Delhi North Campus, University of Delhi, Delhi-110007, India;
H. Suk Advanced Photonics Research Institute, Gwangju Institute of Science and Technology, 123 Cheomdangwagi-ro, Buk-gu, Gwangju, 61005, South Korea; Department of Physics and Photon Science, Gwangju Institute of Science and Technology, 123 Cheomdangwagi-ro, Buk-gu, Gwangju, 61005, South Korea; e-mail: hysuk@gist.ac.kr

Received 6 January 2019; revision received 28 March 2019
Kvantovaya Elektronika **49** (8) 788–795 (2019)
Translated by N.A. Raspopov

centrated between a positively charged ion layer and negatively charged layer of displaced electrons, these layers uniting at a certain distance from the laser pulse axis.

The radiation efficiency at high-power pulse incidence onto a target can be considerably increased by using nanoclusters, nanorods (nanotubes) or nanofilm strips of limited width. In this case, electrons forced out from the target may coherently emit in perpendicular directions at an initial stage of acceleration substantially enhancing the emission conditions. An advantage of such targets is a possibility of simultaneous generation of unipolar and quasi-unipolar radiation pulses (that is, pulses comprising approximately one oscillation period, in which the half-wave of one polarity has the amplitude substantially exceeding that of the other polarity). In generation of unipolar pulses, the pulse amplitude can be substantial due to synchronous summation of the radiation fields from various parts of the target.

In the present work, we study generation of unipolar pulses in the terahertz and IR ranges in the case of high-power non-adiabatic laser pulse incidence to a nanoscale target. For such a target, we have chosen a nanofilm strip of thickness 10 nm with a width of 0.1λ or 4λ, where $\lambda = 1$ μm is the laser radiation wavelength. The employment of two different types of targets with the widths substantially less and greater than wavelength λ gives a chance to study coherently addition of radiation fields of separate electrons. The physical mechanism is suggested and numerically studied, which may lead to generation of unipolar pulses of electromagnetic radiation. The characteristics of such pulses have been found by numerical simulation, in particular, dependences of pulse amplitude and duration on the angle between the radiation propagation direction and laser beam axis. It has been established that in modern laser installations, the amplitudes of unipolar pulses may reach relativistic values (electrons in the fields of such pulses acquire a velocity close to the velocity of light already in time intervals shorter than the pulse duration). In addition, the process of unipolar pulse reflection from an ideally reflecting surface has been numerically analysed, and it has been shown that the pulse holds its unipolar profile.

2. Unipolar pulse generation under synchronous shift of target electrons under the action of a laser pulse

Unipolar pulse generation was studied by 2D numeric simulation using a completely relativistic code XOOPIC [23]. The laser pulse had a duration of three oscillation periods and was non-adiabatic, that is, the amplitude of the first half-wave was approximately the maximal pulse amplitude. In modelling, the pulse linearly polarised along the z axis propagated along x axis (the beam axis crosses the target centre, $y = 30\lambda$). The field distribution along the transverse direction was Gaussian with a beam diameter of 20λ (at the field level 1/e), and the dimensionless field amplitude was $a_0 = 10$. Hereinafter, the dimensionless field amplitude is defined according to the expression $a_0 = eE_0/(mc\omega)$, where E_0 is the dimensional amplitude of the laser pulse or the radiation field amplitude; ω is the laser pulse frequency corresponding to wavelength λ; e and m are the absolute values of electron charge and rest mass, respectively; and c is the speed of light in vacuum. The target centre had the coordinates $x = 20\lambda$, $y = 30\lambda$; the target width was 100 nm, its thickness was 10 nm, and the initial electron concentration was $n = 70n_{cr}$, where $n_{cr} = m\omega^2/(4\pi e^2)$ is the critical concentration (in modelling, it was assumed that the target transfers to the ionised state at the instant of laser pulse arrival and plasma is cold and collision-free). The cell size was $5.1 \times 10^{-3}\lambda$ along the x and y axes, each cell containing 2500 particles (further reduction of the cell size and increase in the number of particles increased the calculation time rather than noticeably affected the modelling results). The ion mass m_i in modelling was taken $1840m$.

A distribution of the radiation field component E_x in the interaction of the laser pulse with the target is presented in Fig. 1a. After interaction, the target is positively charged because all electrons are forced out from it already in a time substantially shorter than the field half-period and are shifted to the right by the laser pulse (one can see a static field of the target near the point $x = 20\lambda$, $y = 30\lambda$). It follows from Fig. 1a that the radiation field is a spherical wave (cylindrical in the case of 2D modelling), which propagates from the target with a decreasing amplitude, all radiation parameters (the wave amplitude, pulse duration and profile) varying along the pulse front. In Fig. 1b, one can see a profile of the field component E_x along the straight line crossing the target in parallel with the y axis after 20 field periods from the start of the interaction. Similar unipolar pulses pass from the target up and

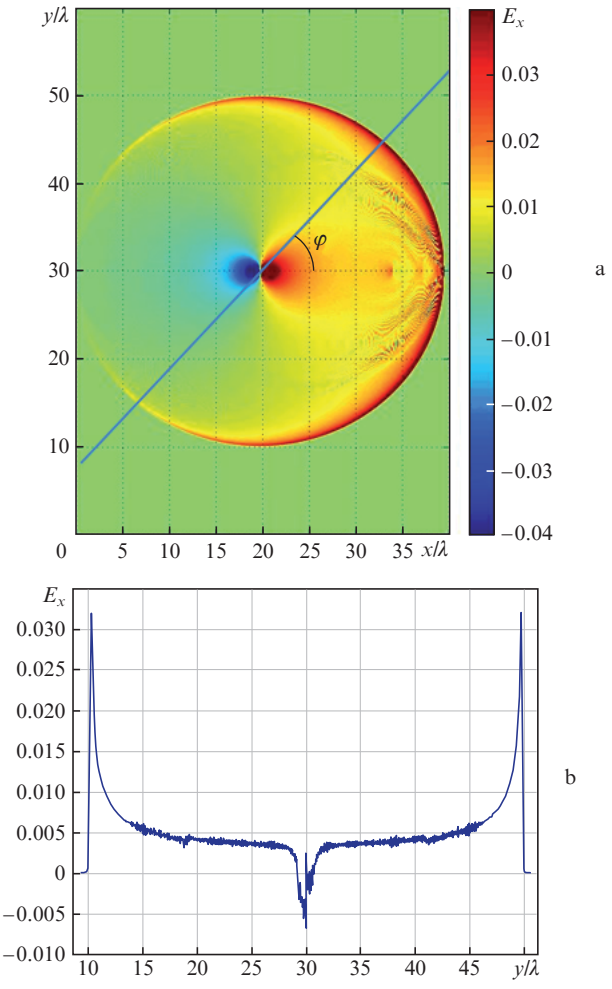

Figure 1. (Colour online) Radiation field for a laser pulse incident onto a target in 20 periods after the start of interaction: (a) spatial distribution of the E_x field component and (b) profile of this component along the line crossing the target parallel to the y axis.

down (Fig. 1a). The width (FWHM) of the pulses depends on the angle φ from the laser beam axis and for vertical propagation it is ~ 0.55 laser field periods.

In 2D modelling, depending on the polarisation of laser radiation, the pulse may efficiently interact with a point target similarly to the interaction with a nanorod or to the interaction with a nanocluster [17]. Indeed, if the laser pulse is polarised along the z axis, the electric field is directed along the nanorod (modelling is two-dimensional and the target is infinite along the z axis) and a current may arise already at small amplitudes, which will result in scattered radiation. If the laser pulse is polarised along the y axis, then the field is directed perpendicular to the target that is equivalent to a cluster in this case; at small amplitudes, the current is absent and emission occurs only when the field increases so that electrons are forced out from the nanorod in the direction of the x axis. In both the cases, when the target interacts with a non-adiabatic pulse of sufficiently high amplitude, a single emission pulse will be formed with a unipolar shape [17].

3. Dynamics of motion of target electrons in generation of unipolar pulses

Dynamics of target electrons was more thoroughly studied in the case of unipolar pulse generation by the laser radiation polarised along the y axis. In this case, the time profile of the laser pulse was Gaussian with the full duration equal to two field oscillation periods (with respect to the field level 1/e). All the rest parameters of the laser pulse and target were the same as in the modelling, which results are presented in Fig. 1. For the target parameters chosen, the laser pulse amplitude is sufficiently large in order to form a single radiation pulse corresponding in shape to the pulse from Fig. 1b. Electron distributions in space at four different instants (two, three, four, and six periods of the laser field after the start of the interaction) obtained from 2D modelling are shown in Fig. 2.

Prior to arrival of the laser pulse half-wave with the amplitude close to maximal one, almost all electrons remain near ions (Fig. 2a, before the interaction, the target resided at the point $x = 6\lambda$, $y = 20\lambda$). This half-wave arrives two periods after the interaction starts, simultaneously forces out all electrons from the target, and electrons begin accelerate mainly in the direction of the laser pulse wavevector, because $a_0 = 10$ and the pulse has a relativistic intensity.

Already during the first (since the start of acceleration) field period, the dense electron bunch covers a distance of $\sim 0.8\lambda$ along the x axis (Fig. 2b). At the initial acceleration stage, when electron velocities are sub-relativistic and the electron bunch size is less than 0.1λ (Fig. 2a), all electrons from the bunch coherently emit, the most intensive emission

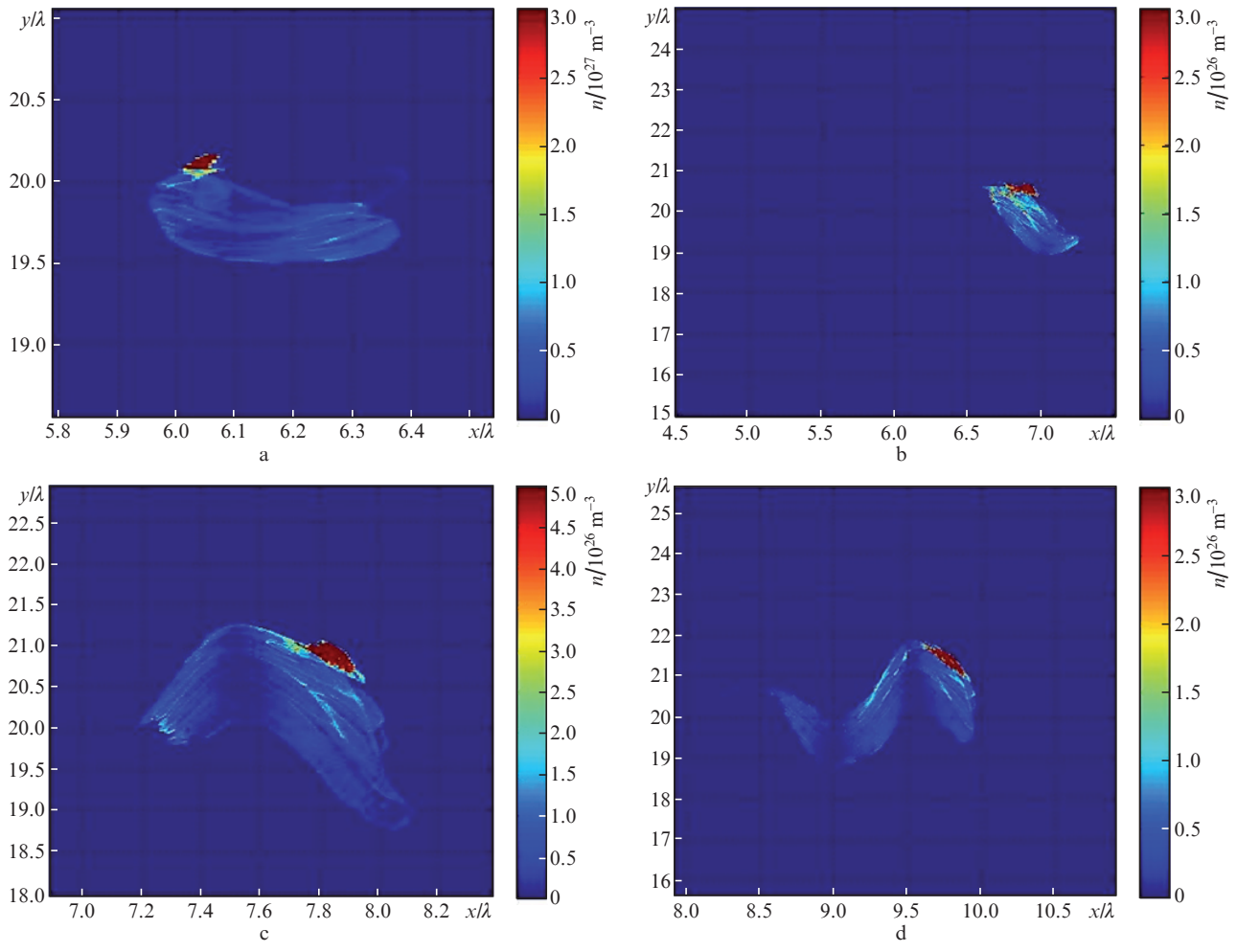

Figure 2. (Colour online) Electron concentration distribution in space at laser pulse incidence onto the target after (a) two, (b) three, (c) four and (d) six laser field periods since the start of the interaction (image contrast is increased for better viewing a dense electron bunch).

is in the direction perpendicular to that of motion. In further motion, longitudinal velocities of bunch electrons become relativistic, and per each period of the field, the x coordinate of the bunch increases by almost a wavelength (Figs 2c and 2d). In this case, the shift in the direction of the laser pulse field (in a transverse direction) during four periods is only one wavelength (from $y \approx 20\lambda$ in Fig. 1a to $y \approx 21\lambda$ in Fig. 2d). The size of the dense electron bunch in the process of motion slightly increases (to 0.2λ after two periods and 0.3λ after four periods). As a relativistic velocity is attained, the bunch electrons, first, coherently emit in a direction close to the direction of motion, which actually coincides with the wave-vector of accelerating laser radiation for large field amplitudes. However, the bunch size continues increasing, the coherence of electron emission worsens, and the efficiency of adding the fields from different electrons substantially falls. Thus, in the vertical direction, only a single pulse is emitted with a duration of approximately half the laser field period; this occurs at the initial moment of dense electron bunch acceleration (see Fig. 1).

Numerical simulation shows that relativistic motion of the bunch along the x axis still continues for at least several tens of periods of the laser field. During this time, the bunch spreads due to Coulomb repulsion between electrons, its density falls and dimensions increase. Part of electrons start to turn back due to ion attraction, this process being asynchronous in contrast to the synchronous acceleration at the beginning, because the first electrons that start to turn back are those the most close to bunch ions for which the Coulomb force is the strongest. Then, the following electrons turn back and so on. While stopping and turning back to a positively charged target, bunch electrons generate the pulses of opposite polarity (as compared to synchronously emitted pulse), which now add incoherently; hence, their total intensity is substantially lower than that of coherently added pulses emitted by electrons at the instant of their departure from the target. From Fig. 2, one can see that during the initial acceleration, there are also electrons, whose motion is asynchronous with that of the bunch (light-blue domains in Fig. 2), and even backward motion to the target is possible. However, the concentration of such electrons is low, and the occupied domain has characteristic dimensions equal to half the wavelength and more; hence, the radiation emitted by these electrons is weak. Thus, the interaction of high-power laser pulses with nanoscale targets may result in generating emission in the form of an unipolar pulse. Note that for an insufficient amplitude of the laser pulse, the asynchronous electron motion may result in forming a quasi-unipolar pulse when a noticeable spike of opposite polarity arises.

Characteristics of the generated emission substantially depend on the dynamics of electron motion in the field of a laser pulse and in Coulomb field of ions. In particular, electrons can be totally forced out from the target only if the pulse amplitude exceeds a certain threshold value [18, 19]. In addition, synchronism of electron motion at the initial acceleration stage is higher for laser pulses with a sharper edge; for pulses with the pulse-rise time substantially shorter than the wave period (non-adiabatic pulses), synchronism is almost perfect. In the latter case, the amplitude of emitted radiation increases. In the result, short laser pulses with a sharp leading edge are preferable for generating such radiation, which is confirmed by results of the numerical simulation.

4. Angular dependence and amplitude of unipolar radiation pulses in the case of wide targets

Characteristics of an emitted unipolar pulse substantially depend on the angle of its propagation direction relative to the laser pulse axis. Pulses emitted at various angles are presented in Fig. 3 for a point target similar to that used in the modelling, whose results are shown in Figs 1 and 2. As the angle increases, the pulse duration becomes first longer and then shorter, the amplitude monotonously falls. Note that in a direction close to the pulse propagation direction and in the backward direction, the pulse amplitudes substantially differ (see Fig. 1a), which is related to relativistic deformation of the directional pattern of the radiation (electrons have a preferable direction of motion, which coincides with the propagation direction of the laser pulse).

The possibility of forming unipolar radiation pulses in the interaction of a laser pulse with nanoscale targets allows one to substantially increase the amplitude of generated pulses by using a wide strip target (extended along the y axis), that is, due to increasing the target area and, consequently, the charge in accelerated electron bunch. In addition, the pulse duration also increases. Indeed, in the case of a wide target, radiation from more distant parts arrives at the observation point with a delay; however, since the sign of the field is the same, the pulse efficiently extends. The maximal radiation delay will be when it propagates in the direction perpendicular to the laser

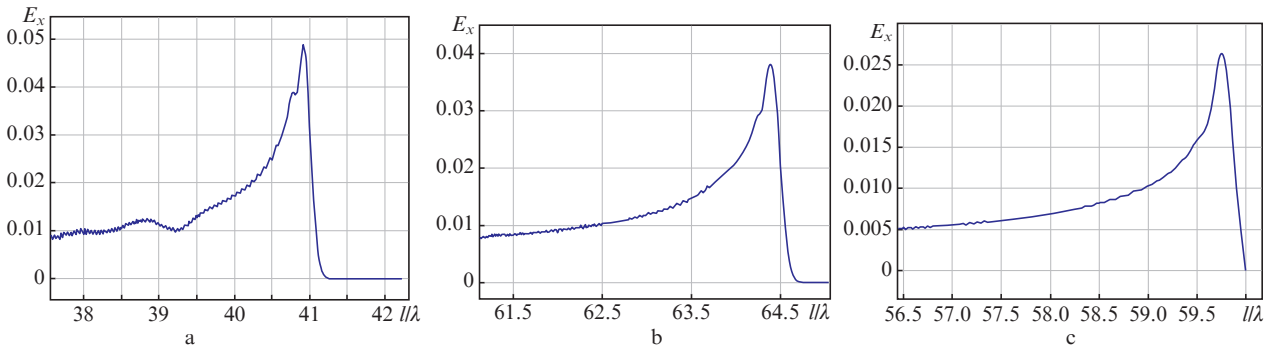

Figure 3. Profiles of the E_x field component for pulses emitted at the angles $\varphi =$ (a) 30°, (b) 60° and (c) 90° relative to the x axis in 30 periods after the start of interaction (the horizontal axis is distance l normalised to λ along the target crossing straight line in Fig. 1a from its left bottom end). Parameters of the laser pulse and target are similar to those in Fig. 1.

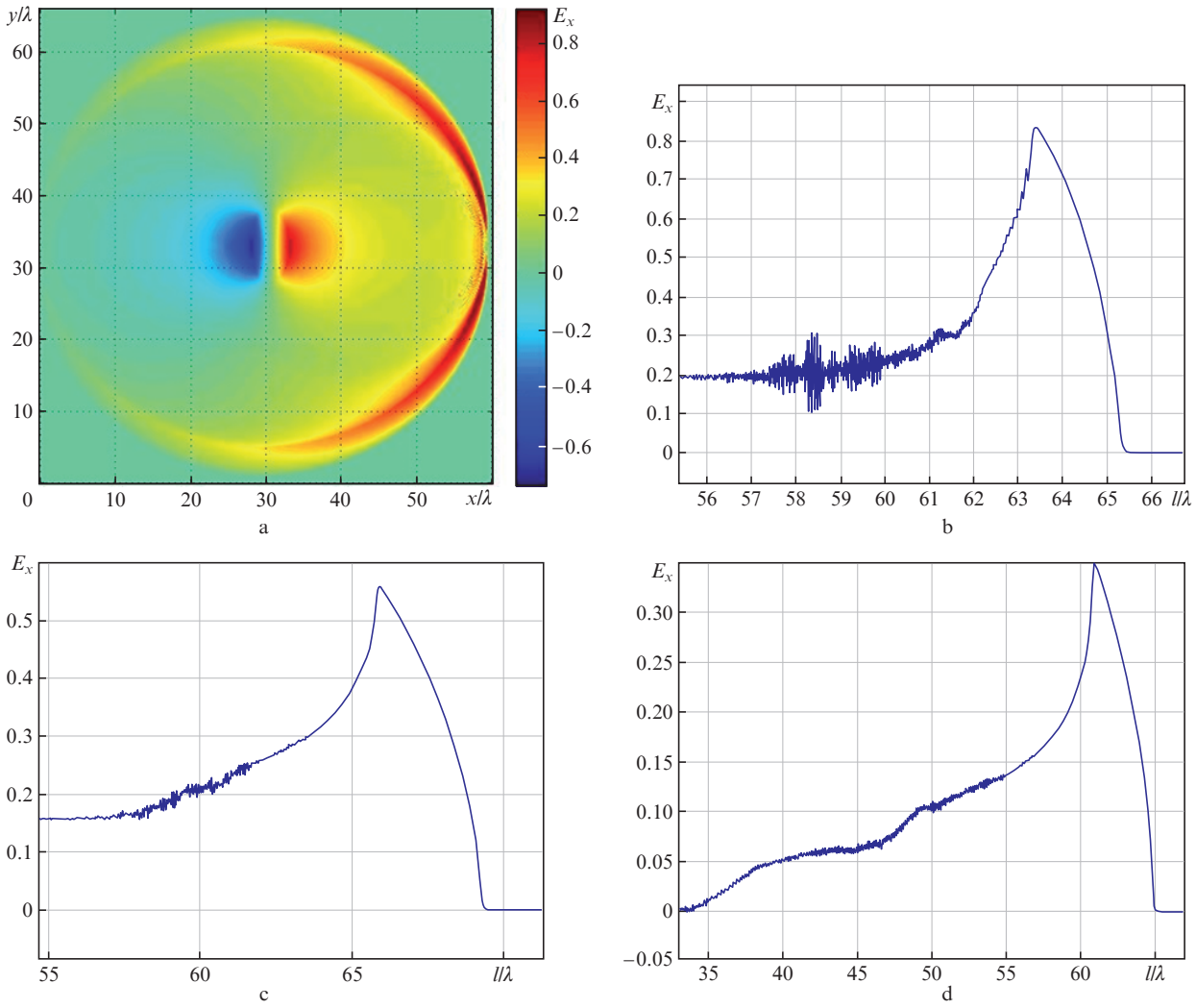

Figure 4. (Colour online) (a) Space distribution of the radiation field component E_x after 30 periods from the start of the interaction and (b–d) profiles of pulses emitted at the angles φ = (b) 30°, (c) 60° and (d) 90° relative to the x axis. The target centre is at point $x = 30\lambda$, $y = 33\lambda$, the rest parameters of the laser pulse and target are similar to those in Fig. 1.

pulse axis, that is, along the x axis. An example of such pulse generation is given in Fig. 4a, where the pulse amplitude reaches relativistic values (teravolts per metre) even at a distance of 30λ from the target; the pulse duration is several periods of the laser field. In this case, the target width (the size along the y axis) is 4λ, and the amplitude of laser pulse required for synchronous electron motion is $a_0 = 30$. The rest parameters of the laser pulse and target are the same as in Fig. 1. Profiles of the pulses emitted at the angles of 30°, 60°, and 90° relative to the x axis are presented in Figs 4b–4d.

In Fig. 5, one can see modulus of the spectrum of the pulse shown in Fig. 4d. The spectrum has a relatively narrow peak at low frequencies and a wide pedestal, which are explained by two different physical processes. The first process is related to sufficiently slowly falling amplitude of the radiation passing from distant target parts with coordinates $z \neq 0$ (in a 2D modelling, the target is infinitely long in the z-axis direction), which results in forming a falling field tail in Figs 4b–4d. The width of this spectral part (FWHM) is ∼6.4 THz (the total width of the principal lobe is 13 THz). The second process related to summation of fields from the target parts (of width 4λ) residing at $z = 0$ has a substantially wider spectrum with

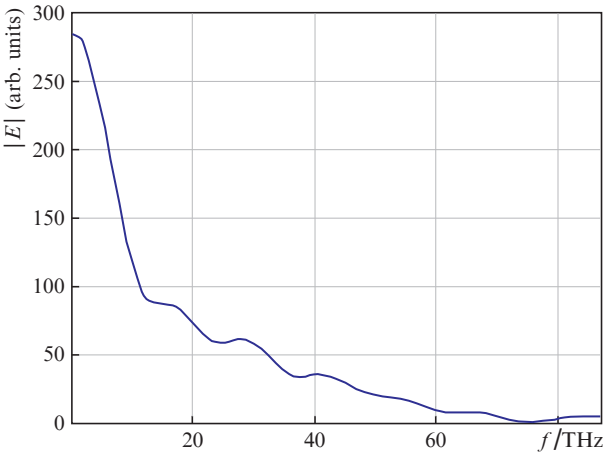

Figure 5. Modulus of a spectrum of the pulse shown in Fig. 4d.

the FWHM of ∼32 THz, which corresponds to the upper terahertz range (the total width of the principal lobe of this part is 74 THz). The FWHM duration of the pulse in Fig. 4d

is 20.5 fs, and the product of the bandwidth to pulse duration is 0.65, which is typical for pulses without high-frequency filling. Nevertheless, note that the spectrum amplitude of such pulses has a finite value at low frequencies, and radiation with frequencies substantially lower than 32 THz can be separated by corresponding filters. Spectra of pulses in Figs 4b and 4c are similar to the spectrum of Fig. 4d, the width of the wideband spectrum part varying according to the pulse duration.

Amplitudes and durations (E_x field component) of generated pulses for the modelling, results of which are shown in Figs 3 and 4, are presented in Fig. 6 as functions of angle φ from the pulse axis. In both the cases, the amplitude of the generated unipolar pulse falls monotonically as the angle increases. At the same time, for a narrow target, the pulse duration has a maximum near $\varphi = 45°$ (Fig. 6a), and for a wide target the pulse duration increases monotonically with the angle due to addition of radiation fields from different target parts and exceeds six laser radiation periods at $\varphi = 90°$ (Fig. 6b). The formation of such a pulse requires a petawatt-level power, which has been realised long ago in high-power laser installations. Further increase in a target width will provide a greater amplitude and duration of the generated unipolar pulse.

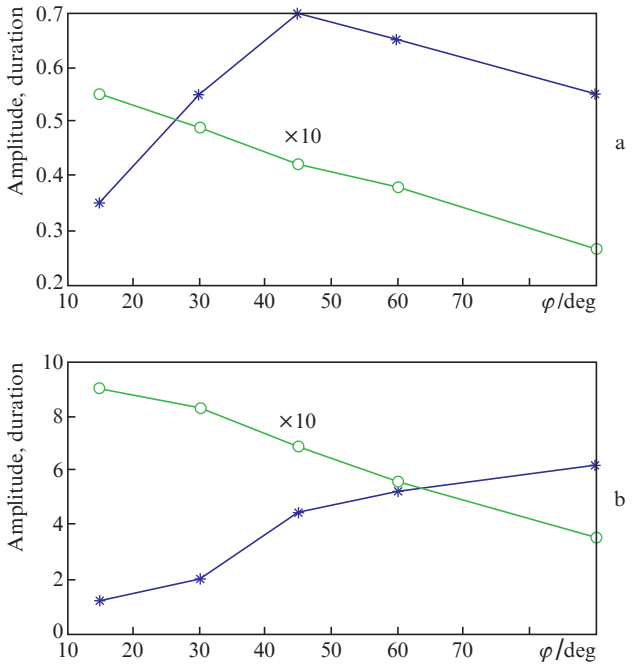

Figure 6. Dimensionless amplitudes (○) and durations (normalised to the laser field period; ✱) of generated pulses vs. angle φ from the laser beam axis for the modelling results presented in (a) Figs 1, 3 and (b) Fig. 4b.

The factor of energy conversion from laser radiation to generated pulse (energy efficiency of the process) depends on the requirements to parameters of such pulses. Having in mind the generation of unipolar pulses with the longest duration, we can estimate the energy of generated radiation in the angle interval 45°–90° relative to the laser beam axis because the duration of pulses generated in this interval varies slightly according to Fig. 6b. Taking into account the 2D character of our modelling and that the laser pulse is not adiabatic, in view of the fact that the radiation passes up and down (see Fig. 4a), we obtain the conversion factor of ~ 1.3% for the angle interval mentioned above and for a target of width 4λ. Since the radiation is formed at the front of a laser pulse, the duration of the latter may be reduced as compared to the modelling value (3λ); in addition, the laser beam diameter can be reduced, which will increase the energy efficiency of the generation process.

Thus, from Figs 4–6, one may conclude that in the interaction of high-power laser pulses with strip targets, radiation pulses with a duration much longer than the laser field period can be generated. At a sufficiently large width of the target, such pulses with a relativistic amplitude correspond to the IR or terahertz ranges. The efficiency of generating such pulses calculated from the generated energy may reach units of percent.

5. Reflection of unipolar electromagnetic pulses from an ideally conducting surface

In applications, rather important is the possibility to form the front of a unipolar electromagnetic pulse and vary the direction of its propagation, in particular, by means of focusing. Reflection of a unipolar electromagnetic pulse with a plane phase front from an ideally conducting surface is numerically analysed below. The modelling was performed in a 2D rectangular domain. Conditions of the zero tangential component of an electric field component are fulfilled at upper and lower boundaries of the domain. The permittivity and magnetic permeability inside this domain are unity (vacuum). A unipolar pulse with a plane front propagates along the x axis from the left boundary (Fig. 7). The pulse polarisation is such that only H_z component of the magnetic field is distinct from zero. Near the right boundary, a conducting wedge is placed with transverse (along the y axis) and longitudinal (along the x axis) sizes substantially greater than the length of the incident pulse along the x axis.

Let us find a spatiotemporal configuration of the field reflected from the wedge. This problem is solved by numerical simulation using the algorithm based on finite-difference approximation of Maxwell's equations in the differential form. For convenience, in this section, time is normalised to the duration of an incident pulse τ, determined with respect to half the maximal amplitude; the spatial coordinate is normalised to the value $c\tau$.

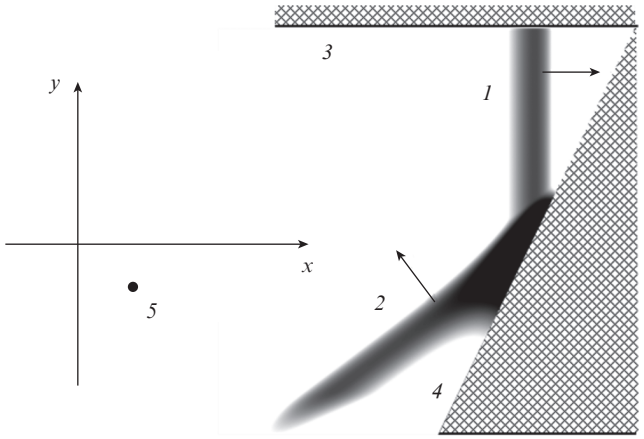

Figure 7. Spatial distribution of the magnetic field at a fixed instant: (*1*) incident pulse; (*2*) reflected pulse; (*3*) upper boundary of a simulation domain; (*4*) ideally conducting inclined plane; (*5*) observation point; arrows show propagation directions for the incident and reflected pulses.

In Fig.7, a spatial distribution is presented for the magnetic field component H_z of a unipolar pulse at a fixed instant when the pulse is near the right top angle of the simulation domain. As follows from Fig. 7, the incident angle of the unipolar pulse equals the angle of reflection. Figure 8 presents the time dependence of the component H_z at the observation point (*5*) in Fig. 7 distant from the reflecting surface by $\sim 7c\tau$. According to Fig. 8, in reflection from the ideally conducting surface, the unipolar pulse holds its time profile, that is, the reflected pulse is unipolar as well. A reduction of the amplitude of the reflected pulse (*2*) as compared to pulse *1* in Fig. 8 is related to the choice of the observation point (*5*).

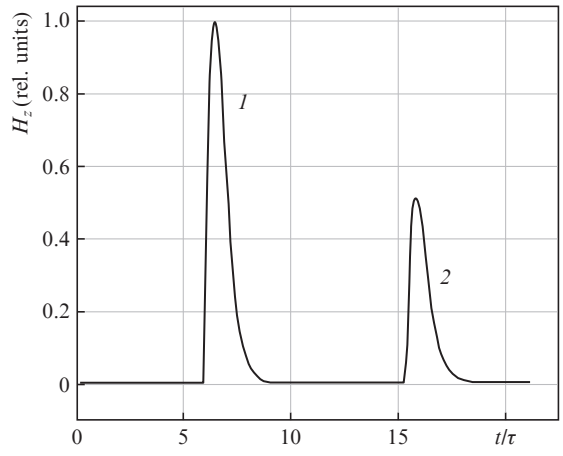

Figure 8. Dependences of the magnetic field for (*1*) incident and (*2*) reflected pulses on time at a fixed observation point (*5*) (see Fig. 7).

Thus, in the considered case, the spatiotemporal configuration of the reflected field is similar to that of the initial pulse. If a focusing surface is used (parabolic and spherical mirrors and so on), the reflected pulse will also be focused, which will provide a concentration of terahertz radiation in a wide angle. Note that conventional optical elements (lens, prism, and so on) cannot be employed in the case of unipolar pulses, because propagation of such pulses in a medium possessing frequency dispersion of permittivity destroys the unipolar structure of pulses in a very short time.

6. Discussion of results and conclusions

Experimental realisation of the scheme suggested for generating unipolar pulses in terahertz and IR ranges by a high-power laser pulse falling onto a nanoscale target requires the fulfilment of several conditions. First, the target should be appropriately placed and fastened in order to make the interaction with the laser pulse most efficient. This problem has been solved already for nanofilms and nanorods (nanotubes). For single clusters (not for a system of chaotically placed clusters), a solution has not been found yet. Second, the laser pulse should have a sufficiently high contrast in order to provide a non-ionised state of the nanoscale target prior to the arrival of the laser half-wave possessing the maximal intensity. This problem has also been solved experimentally by using plasma mirrors, which allow one to increase the contrast of the initial laser pulse by several orders in magnitude. Plasma mirrors are now employed in many laser installations of terawatt power. Finally, the laser pulse should be relativistic and have a sufficiently sharp leading edge. Schemes for generating short relativistic laser pulses (with a duration of about two field periods and less) have already been suggested and experimentally verified; however, the pulse amplitudes are relatively small yet ($a_0 \lesssim 10$). An alternative approach is the employment of methods for sharpening the leading edge of high-amplitude laser pulses based, for example, on nonlinear transparency of the target. However, results of only analytical calculations and numerical modelling are available in this field; the approach itself needs experimental approval.

Thus, in this work, the scheme for generating unipolar pulses in the IR and terahertz ranges is suggested and analysed basing on the interaction of high-power non-adiabatic laser pulse with a nanoscale target (a nanofilm strip with a width from a fraction to several λ). The physical mechanism is considered and numerically studied, which may lead to the formation of unipolar pulses of electromagnetic radiation. The characteristics of such pulses for various target widths have been found by numerical simulation, in particular, dependences of pulse amplitude and duration on the angle between the emission direction and laser beam axis. It has been shown that one can control the pulse duration by varying the target width; in modern laser installations, the amplitudes of unipolar pulses may reach relativistic values (the field intensity is approximately several teravolt per meter). In addition, the reflection of a unipolar pulse from an ideally conducting surface has been numerically analysed and it has been shown that the pulse profile in this case holds its unipolar shape. Quasi-unipolar terahertz pulses of high amplitude may be efficiently used for accelerating electrons and ions, including the formation of a composite accelerating field in conjunction with the laser pulse.

Acknowledgements. H. Suk is grateful to the National Research Foundation of Korea (Project NRF-2017R1A2B3010765) for support.

The research was supported by the Presidium of the Russian Academy of Sciences [Programme No. 9, Research Direction 9.1 Terahertz Optoelectronics (Study of new principles for terahertz radiation generation and detection in radio astronomy, biological, medical, and other applications)].

References

1. Ferguson B., Zhang X.C. *Nat. Mater*., **1**, 26 (2002).
2. Williams G.P. *Rep. Prog. Phys*., **69**, 301 (2006).
3. Reimann K. *Rep. Prog. Phys*., **70**, 1597 (2007).
4. Uryupin S.S., Frolov A.A. *Quantum Electron.*, **43** (12), 1132 (2013) [*Kvantovaya Elektron.*, **43** (12), 1132 (2013)].
5. Mironov V.A., Oladyshkin I.V., Fadeev D.A. *Quantum Electron.*, **46** (8), 753 (2016) [*Kvantovaya Elektron.*, **46** (8), 753 (2016)].
6. Hamster H., Sullivan A., Gordon S., et al. *Phys. Rev. Lett*., **71**, 2725 (1993).
7. Carr G.L., Martin M.C., McKinney W.R., et al. *Nature*, **420**, 153 (2002).
8. Sheng Z.M., Mima K., Zhang J., Sanuki H. *Phys. Rev. Lett*., **94**, 095003 (2005).
9. Wu H.-C., Sheng Z.-M., Zhang J. *Phys. Rev. E*, **77**, 046405 (2008).
10. Jahangiri F., Hashida M., Nagashima T., et al. *Appl. Phys. Lett*., **99**, 261503 (2011).
11. Wu H.-C., Meyer-ter-Vehn J., Ruhl H., Sheng Z.-M. *Phys. Rev. E*, **83**, 036407 (2011).
12. Li Y.T., Li C., Zhou M.L., et al. *Appl. Phys. Lett*., **100**, 254101 (2012).
13. Gopal A., Herzer S., Schmidt A., et al. *Phys. Rev. Lett*., **111**, 074802 (2013).

14. Kuratov A.S., Brantov A.V., Aliev Yu.M., Bychenkov V.Yu. *Quantum Electron.*, **46** (11), 1023 (2016) [*Kvantovaya Elektron.*, **46** (11), 1023 (2016)].
15. Gupta D.N., Kulagin V.V., Suk H. *Opt. Commun.*, **401**, 71 (2017).
16. Kulagin V.V., Kornienko V.N., Cherepnin V.A. *Uchenye Zap. Fiz. Fak. Mosk. Univ.*, No. 4, 144337 (2014).
17. Kulagin V.V., Kornienko V.N., Cherepnin V.A., Gupta D.N. *Zh. Radioelektron.*, No. 1 (2017); http://jre.cplire.ru/jre/jan17/15/text.pdf.
18. Kulagin V.V., Cherepenin V.A., Hur M.S., Suk H. *Phys. Rev. Lett.*, **99**, 124801 (2007).
19. Kulagin V.V., Cherepenin V.A., Gulyaev Y.V., et al. *Phys. Rev. E*, **80**, 016404 (2009).
20. Kiefer D., Henig A., Jung D., et al. *Eur. Phys. J. D*, **55**, 427 (2009).
21. Paz A., Kuschel S., Rodel C., et al. *New J. Phys.*, **14**, 093018 (2012).
22. Kiefer D., Yeung M., Dzelzainis T., et al. *Nat. Commun.*, **4**, 1763 (2013).
23. Verboncoeur J.P., Langdon A.B., Gladd N.T. *Comput. Phys. Commun.*, **87**, 199 (1995).